Proceedings of DETC'04
ASME 2004 Design Engineering Technical Conferences and
Computers and Information in Engineering Conference
September 28-October 2, 2004, Salt Lake City, Utah USA

DETC2004-57441

DESIGN AND CONTROL OF PATH-FOLLOWING COMPLIANT MECHANISMS

Colby C. Swan, Ph.D
Wheeler Faculty Fellow of Engineering
Civil & Environmental Engineering
Center for Computer-Aided Design
The University of Iowa, Iowa City, Iowa
52242, USA

Salam F. Rahmatalla, Ph.D.
Civil & Environmental Engineering
Center for Computer-Aided Design
The University of Iowa, Iowa City, Iowa
52242, USA

Abstract

A control algorithm to manipulate the input actuation forces on hinge-free compliant mechanism models synthesized utilizing continuum topology optimization formulations is implemented and successfully tested in this work, such that the mechanisms follow their specified trajectories and nearby trajectories with high degree of accuracy even when confronted with different resistance forces. The validity of the proposed formulations is tested and demonstrated on number of practical problems involving finite deformation.

1. INTRODUCTION

While rigid-body mechanisms (Fig1.a) can be optimal in innumerable macroscopic mechanical systems, they are generally less suited for micro-scale applications due to the fundamental difficulty of fabricating reliable hinged-joints on such small scales. One potential answer to this problem is to employ compliant mechanisms [1] in which force and motion are transmitted primarily via elastic deformation of the system. The elastic deformation of compliant mechanisms can be either concentrated in flexible hinge regions (Fig. 1b) [2], or it can be more or less uniformly distributed throughout the mechanism (Fig. 1c)[3]. In the former case, an attempt is usually made to re-design the hinged joints of rigid-body mechanisms as flexible hinges in such a way that the performance of the resulting compliant mechanism is roughly comparable to that of the rigid-body mechanism. This is a nontrivial endeavor, however, as designing flexible hinges in a way that permits only rotation at the joint, and so that the material in the hinge is not overstressed or overstrained is very challenging. For these reasons, compliant mechanism designs that feature distributed elastic deformation may be more designable and also more durable.

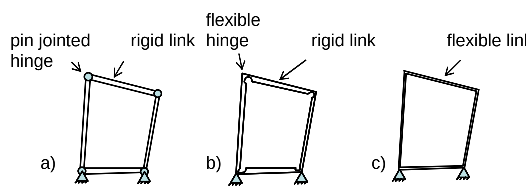

Figure 1. Schematic drawing of generic mechanisms, a) pin-jointed rigid-link mechanism; b) pseudo-rigid link mechanism (compliant hinges substitute for pin-jointed hinges); and c) hinge-free distributed deformation compliant mechanism.

Continuum structural topology design methods have in recent years been investigated quite actively in the design compliant mechanisms, beginning with the seminal work of Ananthasuresh *et al* [4]. Since continuum topology design methods solve for the layout of structural material in continuum structures and mechanical systems, it is somewhat ironic that when applied to design of compliant mechanisms, they have a tendency to produce systems that function as pseudo-rigid-body mechanisms. Such pseudo-rigid-body mechanisms generally feature de facto hinge regions, which are artifacts that behave as hinges. Achieving compliant mechanism designs free of de facto hinges within a continuum topology optimization framework has been addressed previously where it has been observed that such designs generally function as distributed deformation compliant mechanisms.

Since the material comprising compliant mechanisms will generally undergo finite strains, displacements, and rotations when the mechanism functions under normal design actuation forces, the analysis and design framework must be general enough to treat finite deformation effects. One important class of applications among compliant mechanisms are so-called path-following mechanisms in which the output ports of the mechanisms follow a specified trajectory under the effect of a sequence of actuation (input) forces. Research on utilizing continuum topology optimization methods to achieve such path-following compliant mechanisms is still in a state of relative infancy and only a small number of papers have been published toward this end (e.g. [5], [6].)

A design and control methodology is introduced here to realize hinge-free compliant mechanism designs that can follow desired curvilinear paths with good precision even when working against varying workpiece resistances. In the approach, hinge-free compliant mechanism designs that have both sufficient flexibility and strong sensitivity of output port response to input port actuation forces are first obtained utilizing a particular continuum topology optimization formulation [7]. The optimal design process is then followed by application of a control algorithm ([8],[9]) to solve for sequences of actuation forces in response to which the mechanism will follow specified curvilinear trajectories when working against varying resistance forces. The proposed control algorithm is implemented within the solution algorithm for finite deformation structural analysis of compliant mechanism designs. This is followed by a number of practical examples to illustrate the validity of the proposed control algorithm.

2. ELEMENTS OF FORMULATION

2.1 Structural Analysis Model

Since the compliant mechanisms being modeled and designed undergo finite displacements, rotations, and strains the analysis framework should accommodate it. Accordingly, the strong form of the nonlinear elliptic boundary value problem to be solved for the structural displacement field is as follows:

Find $\boldsymbol{u}:(\Omega_S \times [0,T]) \mapsto \Re^3$, such that:

$$\tau_{ij,j} + \rho_0 \gamma_j = 0 \quad \text{on } \Omega_S \ \forall t \in [0,T], \tag{1a}$$

subject to the boundary conditions:

$$u_j(t) = g_j(t) \ \text{ on } \Gamma_{gj} \ \text{ for } j=1,2,3, \ \ \forall t \in [0,T] \tag{1b}$$

$$n_i \tau_{ij} = h_j(t) \ \text{ on } \Gamma_{hj} \ \text{ for } j=1,2,3, \ \ \forall t \in [0,T] \tag{1c}$$

Above, $\boldsymbol{\tau}$ denotes the Kirchhoff stress tensor field which is related to the Cauchy stress tensor $\boldsymbol{\sigma}$ via the relation $\boldsymbol{\tau} = J\boldsymbol{\sigma}$, where $J = \det(\mathbf{F})$ and $\mathbf{F}$ is the deformation gradient operator. As is customary, it is assumed that the Lagrangian surface $\boldsymbol{\Gamma} = \overline{\boldsymbol{\Gamma}_{gj} \cup \boldsymbol{\Gamma}_{hj}}$ bounding the Lagrangian structural domain Ω_S admits the decomposition $\Gamma_{g_j} \cap \Gamma_{h_j} = \{\varnothing\}$ for $j=1,2,3$ For a given mesh discretization of Ω_s whose complete set of nodes is denoted η, the subsequent design formulation is facilitated by introducing a subset of nodes η_h at which non-vanishing external forces are applied, and a subset of nodes η_g at which non-vanishing prescribed displacements are applied.

The particular isotropic hyperelastic strain energy function E used here is that of Ciarlet [10] wherein the volumetric (U) and deviatoric (W) strain energy functions are assumed to be decoupled and of the forms:

$$E(\boldsymbol{F}) = U(J) + \overline{W}(\boldsymbol{\theta}) \tag{2a}$$

$$U(J) = \frac{1}{2}K\left[\frac{1}{2}(J^2-1) - \ln(J)\right] \tag{2b}$$

$$\overline{W} = \frac{1}{2}\mu[tr(\overline{\boldsymbol{\theta}}) - 3] \tag{2c}$$

In the preceding expression, J is again the determinant of $\boldsymbol{F}$; K is a constant bulk modulus; μ is a constant shear modulus; $\boldsymbol{\theta} = \boldsymbol{F}\boldsymbol{F}^T$ is the left Cauchy-Green deformation tensor; and $\overline{\boldsymbol{\theta}} = J^{-(2/3)}\boldsymbol{\theta}$ is its deviatoric part. For this model, therefore, the Kirchhoff stress in a material $\boldsymbol{\tau}$ is thus related to deformation quantities as follows:

$$\boldsymbol{\tau} = JU'(J)\mathbf{1} + 2\,\mathrm{dev}\frac{\partial \overline{W}}{\partial \boldsymbol{\theta}} \tag{3}$$

Using standard techniques, the virtual work equivalent of the original problem statement in Eqs. (1) can be obtained in the following form:

$$\int_{\Omega_S} \tau_{ij}\delta\varepsilon_{ij} d\Omega_S = \int_{\Omega_S} \rho_0 \gamma_j \delta u_j d\Omega_S + \int_{\Gamma_h} h_j \delta u_j d\Gamma_h \tag{4}$$

In the expression above, the quantity on the left represents the internal virtual work δW^{int}, and that on the right, the external virtual work δW^{ext}.

Usage of a Galerkin formulation, in which the real and variational kinematic fields are expanded in terms of the same nodal basis functions, and discretization of the time domain into a finite number of discrete time points, leads to the following force balance equations at each unrestrained node A in the mesh as here at the $(n+1)^{th}$ time step:

$$\mathbf{r}_{n+1}^{A} = (\mathbf{f}^{int})_{n+1}^{A} - (\mathbf{f}^{ext})_{n+1}^{A} = \mathbf{0} \tag{5}$$

where

$$(\mathbf{f}^{int})_{n+1}^{A} = \int_{\Omega_S} (\mathbf{B}^{A})_{n+1}^{T} : \boldsymbol{\tau}_{n+1} d\Omega_S \tag{6}$$

$$(\mathbf{f}^{ext})_{n+1}^{A} = \int_{\Omega_S} \rho_0 N^A \boldsymbol{\gamma}_{n+1} d\Omega_S + \int_{\Gamma_h} N^A \mathbf{h}_{n+1} d\Gamma_h \tag{7}$$

In (6), $\mathbf{B}_{n+1}^{A}$ represents the spatial infinitesimal nodal strain displacement matrix $(\mathbf{B}_{n+1}^{A} = \nabla_{x_{n+1}}^{s} N^A(\mathbf{x}))$, and N^A denotes the nodal basis function for the A^{th} node. Under finite deformations, Eq. (5) represents a set of nonlinear algebraic equations that must be solved in an iterative fashion for the incremental displacement field $(\Delta\boldsymbol{u})_{n+1} = \boldsymbol{u}_{n+1} - \boldsymbol{u}_n$ for each time step of the analysis problem. When external forces applied to a structure are independent of its response, the derivative of the i^{th} residual force vector component at the A^{th} node with respect to the j^{th} displacement vector component of the B^{th} node is simply:

$$\mathbf{K}_{il}^{AB} = \int_{\Omega_S} B_{ji}^{A} c_{jk} B_{kl}^{B} d\Omega_S + \int_{\Omega_S} N_{,j}^{A} \tau_{jk} N_{,k}^{B} \delta_{il} d\Omega_S \tag{8}$$

where c_{jk} is the spatial elasticity tensor in condensed form. Assembly of this nodal stiffness operator for all unrestrained nodes *A* and *B* gives the structural tangent stiffness matrix.

To solve for nonlinear deflection responses of hyperelastic structures, Newton iterations (Fig. 2) are usually performed at each load step of the analysis problem. These involve solving for the set of nodal displacements $\boldsymbol{u}_{n+1}$ that satisfy the force-balance equilibrium condition of Eq. (5).

At t_n displacements $\mathbf{u}_n$ satisfying $\mathbf{r}_n = 0$ were obtained.
Increment time : $t_{n+1} = t_n + \Delta t$;
While($n+1 \le n_{\max}$ and $t_{n+1} \le t_{\max}$)
    Dispalcemnt solution iterations (Newton) :
    Initialize : $k = 0; \mathbf{u}_{n+1}^{k} = \mathbf{u}_n + \mathbf{e}_{n+1}$
    Compute initial residual force vector $\mathbf{r}_{n+1}^{k} = \mathbf{r}(\mathbf{u}_{n+1}^{k})$
    While($\|\mathbf{r}_{n+1}^{k}\| \ge \mathbf{r}_{tol}$ and $k \le k_{\max}$)
        Solve linearized system for incremental displacement $\Delta\mathbf{u}_{n+1}^{k+1}$:
            $\mathbf{K}_{n+1}^{k} . \Delta\mathbf{u}_{n+1}^{k+1} = -\mathbf{r}_{n+1}^{k}$
        Update displacement : $\mathbf{u}_{n+1}^{k+1} = \mathbf{u}_{n+1}^{k} + \Delta\mathbf{u}_{n+1}^{k+1}$
        Update residual force vector : $\mathbf{r}_{n+1}^{k+1}(\mathbf{u}_{n+1}^{k+1})$
        $k = k+1$
    End while
    $\mathbf{u}_{n+1} = \mathbf{u}_{n+1}^{k}$
End while

Figure 2 Algorithm for Newton iterations during a representative time/load step $(n+1)^{th}$ of nonlinear structural analysis without control.

2.2 Continuum Topology Optimization

In continuum topology optimization, one frequently solves for the spatial distribution of a fixed volume of structural material in Ω_S such that the desired performance characteristics of the structure are optimized. In the current framework, this is achieved by using the same C^0 bi-linear nodal basis functions of the structural analysis problem to interpolate nodal volumetric densities of structural material throughout the structural domain Ω_S. Specifically, in the infinitesimal neighborhood about a point $\mathbf{X} \in \Omega_S$, the volumetric density of solid structural material $\phi(\mathbf{X})$ is given by

$$\phi(\mathbf{X}) = \sum_{A \in \eta} N_A(\mathbf{X}) \phi_A \tag{9}$$

where the ϕ_A represent nodal volumetric densities of solid material. Since at each point $\mathbf{X} \in \Omega_S$ there is generally a mixture of a solid structural material and a void-like material with respective volume fractions $\phi(\mathbf{X})$ and $1-\phi(\mathbf{X})$ a methodology is generally needed to determine the effective stiffness properties of the solid-void mixture or composite. A number of different possibilities exist, and a fairly detailed review was presented in [10]. Here, a simple iso-deformation powerlaw mixing rule is employed in which it is assumed that both the solid and void-like material at a point $\mathbf{X}$ undergo identical deformations. Accordingly, at each point $\mathbf{X}$, both the solid and void-like materials are assumed to share the same deformation gradient:

$$\mathbf{F}(\mathbf{X}) = \mathbf{F}_{solid}(\mathbf{X}) = \mathbf{F}_{void}(\mathbf{X}) \equiv \frac{\partial \mathbf{x}}{\partial \mathbf{X}}. \tag{10}$$

Although the solid and void-like materials share the same state of deformation, the stress states in each are generally consistent with their own constitutive behaviors. Assuming that both the solid and void-like materials can be represented by the hyperelastic constitutive model of the preceding section it follows that a point $\mathbf{X}$ the stresses in the respective materials would be:

$$\begin{aligned} \boldsymbol{\tau}_{\mathbf{solid}} &= J\mathrm{U}'_{\mathrm{solid}}(J)\mathbf{1} + 2\,\mathrm{dev}\frac{\partial \overline{\mathrm{W}}_{solid}}{\partial \boldsymbol{\theta}}; \\ \boldsymbol{\tau}_{\mathbf{void}} &= J\mathrm{U}'_{\mathrm{void}}(J)\mathbf{1} + 2\,\mathrm{dev}\frac{\partial \overline{\mathrm{W}}_{void}}{\partial \boldsymbol{\theta}} \end{aligned} \tag{11}$$

In accordance with the powerlaw mixing rule the average stress in the solid-void mixture at point $\mathbf{X}$ is just the weighted sum as follows:

$$\boldsymbol{\tau}(\mathbf{X}) = \phi^P(\mathbf{X})\,\boldsymbol{\tau}_{solid} + \left[1 - \phi^P(\mathbf{X})\right]\boldsymbol{\tau}_{void} \tag{12}$$

To achieve the effect of a void-like material in this work, the bulk and shear moduli of the void material are taken to be 10^{-6} times those in the solid structural material. In the mixing rule of Eq. (12), the powerlaw exponent P is generally chosen larger than unity, but less than or equal to four. A value of unity yields the classical Voigt rule of mixtures, whereas a value of $P = 4$ leads to a penalized mixture in which stiffness approaching that of the solid material is achieved only for values of ϕ very close to unity.

In continuum topology optimization, the layout of structural material within Ω_S is iteratively varied, and for each variation, the structure is re-analyzed. The design of such a structure can be represented by a finite dimensional vector $\mathbf{b} \in \Re^N$ wherein each component of the vector represents a nodal volume fraction of solid material, and N denotes the number of nodes in the analysis model at which the design can be varied. Since the nodal volume fractions are continuous on the interval $\phi \in [0,1]$, and since the design of a structure is represented by N such variables, where N can easily be on the order of 10^3 or greater, gradient-based optimization methods are typically most effective for solving continuum structural topology design problems.

A design problem is usually solved by specifying a performance-based objective function $\Im(\mathbf{b})$ for the structure, and searching the design space $\Re^N$ for the design $\mathbf{b}^*$ that optimizes the performance. In gradient-based optimization, it is thus necessary to compute the so-called design derivatives of $\Im$ as follows:

$$\frac{d\Im}{d\mathbf{b}} = \frac{\partial \Im}{\partial \mathbf{b}} + \frac{\partial \Im}{\partial \mathbf{u}} \cdot \frac{d\mathbf{u}}{d\mathbf{b}} \tag{13}$$

Fairly extensive details on computation of design derivatives of performance functionals for hyperelastic structures at finite deformations were provided in [11] and so they are not reproduced here. An algorithmic view of finite deformation structural analysis and design sensitivity analysis embedded within a continuum topology design optimization framework is shown in Fig. 3.

Given a starting material layout $\mathbf{b}_o$

* Initialize $\mathrm{t}_o, \mathbf{u}_o, \dfrac{d\Im}{d\mathbf{b}}$

For$(n = 0; n \le n_{\max}; n++)$

  Increment time : $t_{n+1} = t_n + \Delta t$

  Initialize $k = 0; \mathbf{u}_{n+1}^k = \mathbf{u}_n + \mathbf{e}_{n+1}$

  Compute initial residual force vector : $\mathbf{r}_{n+1}^k = \mathbf{r}(\mathbf{u}_{n+1}^k)$

  While $(\left\|\mathbf{r}_{n+1}^k\right\| \ge r_{tol}$ and $k \le k_{\max})$

    Solve linearized system for incremental displacement $\Delta\mathbf{u}_{n+1}^{k+1}$

    $\mathbf{K}_{n+1}^k . \Delta\mathbf{u}_{n+1}^{k+1} = -\mathbf{r}_{n+1}^k$

    Update displacement : $\mathbf{u}_{n+1}^{k+1} = \mathbf{u}_{n+1}^k + \Delta\mathbf{u}_{n+1}^{k+1}$

    Update residual force vector : $\mathbf{r}_{n+1}^{k+1}(\mathbf{u}_{n+1}^{k+1})$

    $k = k + 1$

  End - while

  $\Delta\mathbf{u}_{n+1} = \mathbf{u}_{n+1} - \mathbf{u}_n$

  $$\begin{aligned} \frac{d(\Delta\Im)_{n+1}}{d\mathbf{b}} &= \frac{\partial(\Delta\Im)_{n+1}}{\partial \mathbf{b}} + \frac{\partial(\Delta\Im)_{n+1}}{\partial(\Delta\mathbf{u})_{n+1}} . \frac{d(\Delta\mathbf{u})_{n+1}}{d\mathbf{b}} \\ &= \frac{\partial(\Delta\Im)_{n+1}}{\partial \mathbf{b}} + \frac{\partial(\Delta\Im)_{n+1}}{\partial(\Delta\mathbf{u})_{n+1}} . \mathbf{K}_{n+1}^k . \frac{\partial(\mathbf{r})_{n+1}}{\partial \mathbf{b}} \end{aligned}$$

  $\dfrac{d\Im}{d\mathbf{b}} = \dfrac{d\Im}{d\mathbf{b}} + \dfrac{d(\Delta\Im)_{n+1}}{\partial \mathbf{b}}$

  $\Im = \Im + \Delta\Im(\Delta\mathbf{u}_{n+1})$

  $\mathbf{u}_{n+1} = \mathbf{u}_{n+1}^k$

End - for

If($\mathbf{b}$ does not satisfy first order optimality conditions or it is not feasible)

  Compute : $\Delta\mathbf{b}\left(\Im, \dfrac{d\Im}{d\mathbf{b}}, \aleph, \dfrac{d\aleph}{d\mathbf{b}}\right)$

  $\mathbf{b} = \mathbf{b} + \Delta\mathbf{b}$

  Return to *

End - if

Figure 3 Algorithm for nonlinear structural analysis and sensitivity analysis embedded within design optimization problem.

2.3 Control Within A Nonlinear Analysis Framework

For a given layout of material within the structural model, it is useful to be able to solve for a sequence of actuation forces $\mathbf{f}_0^{in}, \mathbf{f}_1^{in}, \mathbf{f}_2^{in}, \mathbf{f}_3^{in}, \ldots, \mathbf{f}_N^{in}$ that, when applied to the mechanism's input port, will result in the mechanism's output port moving along a desired trajectory specified by a corresponding sequence of output port displacements: $(\mathbf{u}_0^*)^{op}, (\mathbf{u}_1^*)^{op}, (\mathbf{u}_2^*)^{op}, \ldots, (\mathbf{u}_N^*)^{op}$.

Within a typical single incremental load-step $(n+1)$ of the nonlinear structural analysis problem, one solves a sequence of trial incremental analysis problems with trial actuation forces $\left(\mathbf{f}_{n+1}^{in}\right)^j$, $j = 0,1,2,\ldots$ until the equilibrium output port displacement $\left(\mathbf{u}_{n+1}^{j+1}\right)^{op} \subset \mathbf{u}_{n+1}^{j+1}$ associated with the trial actuation force is as close as possible to the target value for that increment $\left(\mathbf{u}_{n+1}^{*}\right)^{op}$ (Fig.4). In a formal sense, the following optimization problem is solved for the actuation force $\mathbf{f}_{n+1}^{in} \subset \mathbf{f}_{n+1}^{ext} \in \Re^{ndof \times numnp}$ associated with each load step of the structural analysis problem:

For predetermined $\mathbf{f}_n^{in}, \mathbf{u}_n$ find $\mathbf{f}_{n+1}^{in}, \mathbf{u}_{n+1}$ such that

$$\min_{\mathbf{f}_{n+1}^{in}} (g) \ \text{ and } \ \mathbf{r}(\mathbf{f}_{n+1}^{in}, \mathbf{u}_{n+1}) = \mathbf{0} \tag{14}$$

where:

$$g(\mathbf{u}(\mathbf{f}_{n+1}^{in})) = \left\| \mathbf{u}_{n+1}^{op} - \left(\mathbf{u}_{n+1}^{*}\right)^{op} \right\|^2 \tag{15}$$

is the objective function; $\mathbf{u}_{n+1}^{op} \subset \mathbf{u}_{n+1} \in \Re^{ndof \times numnp}$ is the resulting output port displacement due to the actuation force $\mathbf{f}_{n+1}^{in}$; and $\left(\mathbf{u}_{n+1}^{*}\right)^{op}$ is the target output port displacement for the $(n+1)^{th}$ load step.

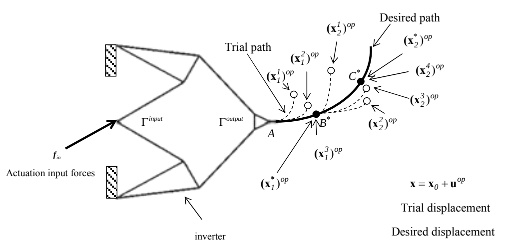

Figure 4 Schematic of iterative control problem for actuation forces that make mechanism output port follow a desired path.

To solve this unconstrained optimization problem within each load step of the nonlinear analysis problem, an iterative conjugate gradient algorithm is employed. For a trial value of the actuation force the gradient of the objective function with respect to the actuation force is computed as:

$$\left(\nabla g\right)_{n+1}^j = -\left(\mathbf{u}^a\right)_{n+1}^j \cdot \frac{d\mathbf{f}^{ext}}{d\mathbf{f}_{n+1}^{in}} \tag{16}$$

where $\mathbf{u}^a \in \Re^{\text{ndof x numnp}}$ is a vector of adjoint displacements satisfying the following linear adjoint problem:

$$\mathbf{K}_{n+1}^{j} \cdot \left(\mathbf{u}^a\right)_{n+1}^j = -\left(\frac{\partial g}{\partial \mathbf{u}}\right)_{n+1}^j \tag{17}$$

in which $\mathbf{K}_{n+1}^j$ is tangent stiffness operator at the current trial equilibrium state of the model associated with $\left(\mathbf{f}_{n+1}^{in}\right)^j$. Once the gradient of the objective function is obtained, the algorithm for obtaining the subsequent trial actuation force (Fig. 5) is followed.

Initialize : time step counter $n = 0$; Initialize time : $t_{n+1} = t_n + \Delta t$;
While $(n+1 \le n_{\max}$ and $t_{n+1} \le t_{\max})$
  Initialize $(\mathbf{u}_{n+1}^*)^{op}$: target output port displacement at t_{n+1}
  Control force iterations :
  Initialize : $j = 0$; $(\mathbf{f}_{n+1}^{in})^{j+1} = \boldsymbol{f}^{trial}$
  * Displacement solution iterations (Newton) :
    Initialize : $k = 0$; $\mathbf{u}_{n+1}^k = \mathbf{u}_n + \mathbf{e}_{n+1}$
    Compute initial residual force vector : $\mathbf{r}_{n+1}^k = \mathbf{r}(\mathbf{u}_{n+1}^k)$
    While $(\|\mathbf{r}_{n+1}^k\| \ge r_{tol}$ and $k \le k_{\max})$
      Solve system for incremental displacement $\Delta\mathbf{u}_{n+1}^{k+1}$:
      $\mathbf{K}_{n+1}^k . \Delta\mathbf{u}_{n+1}^{k+1} = -\mathbf{r}_{n+1}^k$
      Update displacement : $\mathbf{u}_{n+1}^{k+1} = \mathbf{u}_{n+1}^k + \Delta\mathbf{u}_{n+1}^{k+1}$
      Update residual force vector : $\mathbf{r}_{n+1}^{k+1}(\mathbf{u}_{n+1}^{k+1})$
    End - while
  $(\mathbf{u}_{n+1}^{j+1})^{op} = (\mathbf{u}_{n+1}^{k+1})^{op}$
  $g_{n+1}^{j+1} = \|(\mathbf{u}_{n+1}^{j+1})^{op} - (\mathbf{u}_{n+1}^*)^{op}\|^2$
  If $(g_{n+1}^{j+1} \ge g_{tol}$ and $j+1 \le j_{max})$ solve for ∇g_{n+1}^{j+1},
    Find search direction $\mathbf{d}_{n+1}^{j+1}(\nabla g_{n+1}^j, \nabla g_{n+1}^{j+1})$ using conjugate gradient method.
    Find the step size α_{n+1}^{j+1} for the line search.
    $j = j+1$
    $(\mathbf{f}_{n+1}^{in})^{j+1} = (\mathbf{f}_{n+1}^{in})^j + \alpha_{n+1}^{j+1}.\mathbf{d}_{n+1}^{j+1}$
    Jump to *
  End - if
  $\mathbf{u}_n = \mathbf{u}_{n+1}^j$; $n = n+1$; $t_{n+1} = t_n + \Delta t_{n+1}$;
End - while

Figure 5 Algorithm for control problem interleaved with nonlinear analysis problem.

3. CONTINUUM TOPOLOGY DESIGN OF HINGE-FREE MECHANISMS

3.1 Design Problem Formulation

The first objective in the proposed framework is to achieve hinge-free workable compliant mechanism designs that can subsequently be controlled with actuation forces so that the output port follows specified trajectories. In the topology design formulation, usage is made of two distinctly different sets of springs having different purposes. The first set of springs are called *artificial springs* and they are chosen to be very stiff [7]. The second set of springs is called *workpiece springs* and these represent the much smaller resistance supplied by the workpiece when manipulated by the mechanism.

To design a mechanism within the proposed framework, a mathematical mechanism model on a spatial region $\Omega_s \in \Re^3$ is first created and support conditions are prescribed (Fig. 6). An input port region Γ_{in} to which an input force $\mathbf{f}_{in}$ will be applied is identified, as is an output port region Γ_{out} at which $\mathbf{u}_{out}$ is monitored.

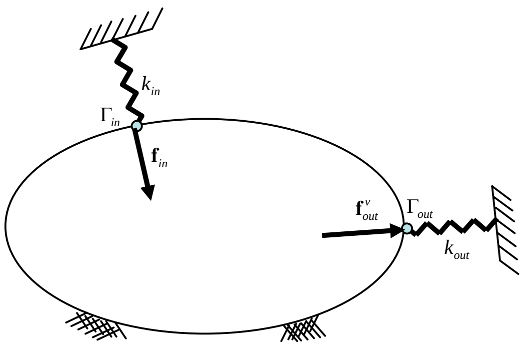

Fig. 6. Schematic of compliant mechanism design problem using artificial springs attached to both input port and output port.

Compliant mechanisms can be designed and fabricated with a wide variety of materials and here the material considered is aluminum ($E = 73\,\text{GPa}$; $\nu = .35$). Typically layout optimization of material in compliant mechanisms utilizing continuum topology optimization is performed with a prescribed amount C of material specified as a fraction $\Im_M$ of the mechanism's envelope volume. For a given design, the ratio of structural material volume to the mechanism's envelope volume V is computed as follows:

$$\Im_M = \frac{1}{V}\int_{\Omega_b} \phi(\mathbf{X})\,\mathrm{d}\Omega\,. \tag{18}$$

To achieve mechanism designs free of *de facto* hinges, the material layout problem is solved to minimizes the sign inverse of the elastic mutual potential energy (MPE) under a given actuation force $\mathbf{f}_{in}$ while working against the stiff *artificial* springs attached to both the I/P and O/P of the mechanism.. Here, the MPE is defined as follows:

$$\mathrm{MPE} = \mathbf{f}^v_{out} \cdot \mathbf{u}^{(1)}_{out} \tag{19}$$

where $\mathbf{u}^{(1)}_{out}$ is the displacement at the output port due to a load $\mathbf{f}_{in}$ applied at the input port, and $\mathbf{f}^v_{out}$ is a virtual force at the output port specifying the direction of the desired output port displacement. A solution of the following optimization problem **P1** is obtained subject to a material usage constraint and existence of an equilibrium solution of the structural equilibrium problem:

P1: For fixed material usage constraint value C and artificial spring stiffnesses k_b:

$$\min_{\mathbf{b}} \left[(\text{-}\,\mathrm{MPE}) + \lambda_1 \left\langle \Im_M - C \right\rangle + \mathbf{u}^a \cdot \mathbf{r}(\mathbf{u},\mathbf{b})\right] \tag{20}$$

where $\mathbf{r} \in \Re^{\text{ndof x numnp}}$ is the residual force vector for the elastic structural model which vanishes when the structure is in equilibrium under the applied actuation forces and the spring reaction forces. Also in the above, λ_1 is the nonnegative Lagrange multiplier associated with the material usage constraint, and $\mathbf{u}^a \in \Re^{\text{ndof x numnp}}$ is a vector of nodal adjoint displacements that serve as Lagrange multipliers to the structural equilibrium equality constraint [12].

It is emphasized design solutions of **P1**, for a specified amount C of structural material, will generally be very stiff. To subsequently model how such mechanism designs function at finite deformations under real workpiece resistance, the stiff artificial springs are removed and the second set of *workpiece* springs are attached only to the O/P of the mechanism. A realistic goal in design of compliant mechanisms is to have the mechanism be free of *de facto* hinges, and to have a complimentary compliance E_C at finite deformation that exceeds a certain threshold value E_C^* when working against the *workpiece* resistance in response to a specified actuation force $\mathbf{f}_{in}$. Here the complimentary compliance E_C of the mechanism is defined as:

$$E_C = \frac{\left\|\mathbf{f}_{in}\right\|}{\left\|\mathbf{f}^v_{out}\right\|}\left(\mathbf{f}^v_{out} \cdot \mathbf{u}^{(1)}_{out}\right) = \frac{\left\|\mathbf{f}_{in}\right\|}{\left\|\mathbf{f}^v_{out}\right\|} * MPE \tag{21}$$

Depending on the material usage constraint value C for which design problem **P1** was solved, the resulting design solution might very well be too stiff with $E_C < E_C^*$. Nevertheless, design problem **P1** can be re-solved with progressively smaller values of the material usage constraint value C until $E_C = E_C^*$. The objective is thus to find the largest value of the material usage constraint value C for which $E_C = E_C^*$. A concise mathematical statement of the extended design problem **P2** that corresponds to this procedure is as follows:

P2: For specified *artificial springs* (k_{in}, k_{out}) and *workpiece springs* $k_{workpiece}$ find:

$$\inf C \in (0,1) \text{ and } \min_{\mathbf{b}\in\Re^N}(-\text{MPE}) \text{ such that:} \quad (22a)$$

$$\Im_M - C \leq 0 \text{; material usage constraint} \quad (22b)$$

$$\mathbf{r}(\mathbf{u}^{(1)}, \mathbf{b}, C) = \mathbf{0} \text{; Case 1 equilibrium} \quad (22c)$$

$$\mathbf{r}(\mathbf{u}^{(2)}, \mathbf{b}, C) = \mathbf{0} \text{; Case 2 equilibrium} \quad (22d)$$

$$E_C^* - E_C(\mathbf{u}^{(2)}, \mathbf{b}, C) \leq 0 \text{; Case 2 compliance} \quad (22e)$$

In **P2**, the Case 1 analysis has stiff springs attached to both the I/P and O/P of the structural model, and the structure is analyzed using linear elastic analysis. The resulting displacement field in the structural model from which *MPE* is computed is denoted $\mathbf{u}^{(1)}$. In Case 2 analysis, the stiff springs are removed from the model's I/P and O/P and moderate workpiece springs are attached to the O/P. The finite deformation hyperelastic response of the structure $\mathbf{u}^{(2)}$ to the actuation force $\mathbf{f}_{in}$ is computed, from which the complimentary compliance is also computed. In Eq. (22e) of **P2**, E_C^* is the target value for complimentary compliance when working against the *workpiece* springs under actuation force $\mathbf{f}_{in}$. The approach taken herein to solve **P2** is to first solve design problem **P1** for numerous values of the material usage constraint C. Each of the designs for different C values is then analyzed at finite deformation under the actuation force $\mathbf{f}_{in}$ and complimentary compliances $E_C(\mathbf{u}^{(2)}, \mathbf{b}, C)$ are computed. The design **b** associated with the material usage constraint value C that yields the target complimentary compliance E_C^* is then selected.

3.2 Design of Hinge-Free Inverter Mechanisms

The function of this device is to have the output port displace in a direction opposite to that of an input force applied at the input port. Fig. 7 shows the design domain Ω_s of the inverter problem with partial fixed support boundaries at the left hand side. The domain, which is discretized with a minimum of 100 x 100 bilinear quadrilateral finite elements, is loaded with $f_{in} = 100N$ applied to the input port. The deflection at the output port in the direction of $\mathbf{f}_{out}^v$ is to be maximized. The large artificial spring stiffness values used on both the input and output ports of the mechanism are $k_b = 1.6 \cdot 10^{10}\,\text{N}\cdot\text{m}^{-1}$.

To demonstrate the effects of material usage constraint on resulting compliant mechanism characteristics, the design problem **P1** was solved with: $C = 0.30$ (Fig. 7b,c); $C = 0.10$ (Fig. 7d,e); and $C = 0.03$ (Fig. 7f,g). Each design functions without any *de facto hinges*, and the more sparse designs feature nicely distributed elastic deformation.

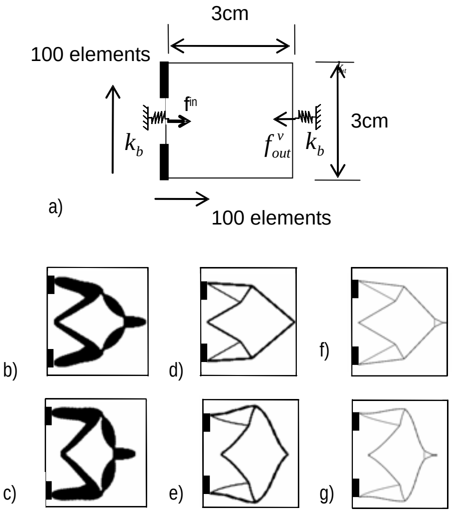

Fig. 7. a) Inverter mechanism design region and loading conditions; b) design solution of **P1** with C=.30; c) deformed configuration; d) design solution for C=.10; e) deformed configuration; f) design solution with C=.03; g) deformed configuration.

If for an actuation force $f_{in} = 100N$ a threshold complimentary compliance $E_C^* = 2 \cdot 10^{-3} J$ is desired when $k_{workpiece} = 10^6 N/m$ then $\inf C = 0.05$ as is shown in Fig. 8.

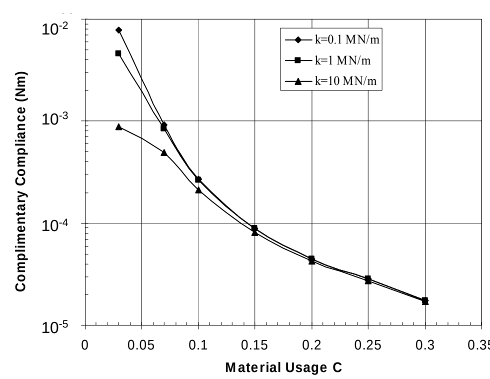

Fig. 8 Computed complimentary compliances of the aluminum inverter mechanism at finite deformation versus material usage factor C for different workpiece spring stiffnesses.

4. INVERTER AS A PATH FOLLOWING COMPLIANT MECHANISM

In the preceding section the inverter mechanisms (Fig. 7) were designed such that their output ports follow a horizontal path under the effect of a horizontal actuation force. The next goal of this work is to test the ability of the proposed control algorithm to solve for actuation forces so that the mechanisms can follow paths close to the originally intended path or even paths not so close to the originally intended path. In all of the control problems solved below, the sparse inverter mechanism design shown in Fig. 7f was utilized.

The mechanism was first controlled to follow a backward horizontal path and then a forward horizontal path in the absence of workpiece resistance (Fig. 9). The required forces to control the mechanism in the backward path are quite linear whereas those required to move the O/P forward are somewhat nonlinear.

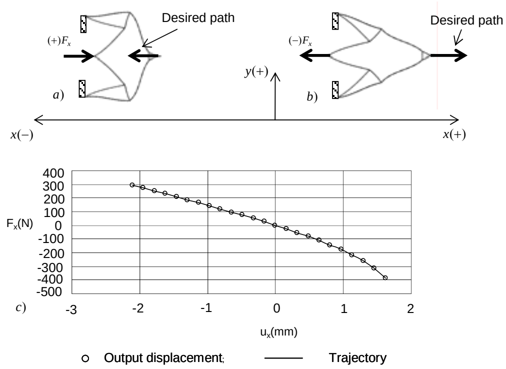

Fig. 9 a) Mechanism is controlled to follow a backward horizontal path; and b) a forward horizontal path; c) graph showing the computed relation between the input force components and the output port displacements.

Next, the mechanism was controlled to follow a backward inclined path and then a forward inclined path (Fig. 10), both in the absence of any workpiece resistance.

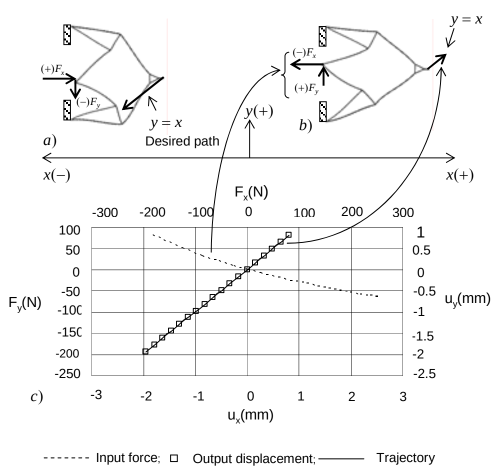

Fig. 10. a) Mechanism when controlled to follow backward inclined path; and b) a forward inclined path; c) graph showing computed relations between actuation force components and output port displacements.

The final control test for the inverter mechanism in the absence of workpiece resistance solved for the actuation forces to move the O/P in a backward parabolic path and then a forward parabolic path (Fig. 11).

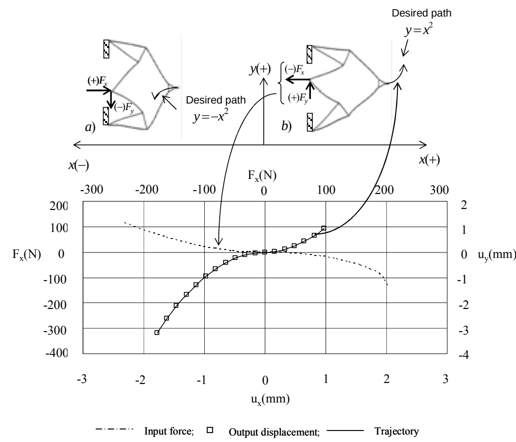

Fig. 11. a) Mechanism when controlled to follow follow forward parabolic path; and b) a backward parabolic path; c) graph showing computed relations between the input forces and output displacements.

Against relatively light workpiece resistance $k = 10^5 N/m$ the mechanism was then controlled to undergo a backward inclined motion, and then a forward inclined motion (Fig. 12). The computed control force versus displacement characteristics of the mechanism are similar to those computed in the absence of any resistance (Fig. 10), although the magnitudes of the necessary control forces are somewhat larger, as would be expected.

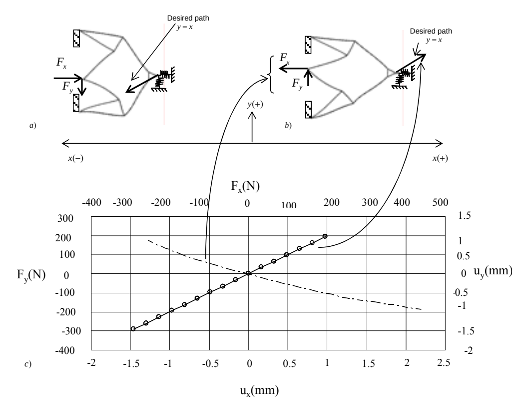

Fig. 12. a) Mechanism when controlled to follow forward inclined path against workpiece springs with stiffness 10^5 N/m; and b) when following a backward inclined; c) graph showing computed relations between input forces and output displacements.

When an attempt was made to make the same sparse mechanism follow a backward and then forward inclined path when working against very stiff workpiece resistance $\left(k = 10^7 N/m\right)$, the mechanism was found to be too compliant. Then the somewhat stiffer inverter mechanism obtained with $\left(C = 0.10\right)$ and shown in Fig. 7d was used with more success. The computed control forces versus O/P displacements are shown in Fig. 13.

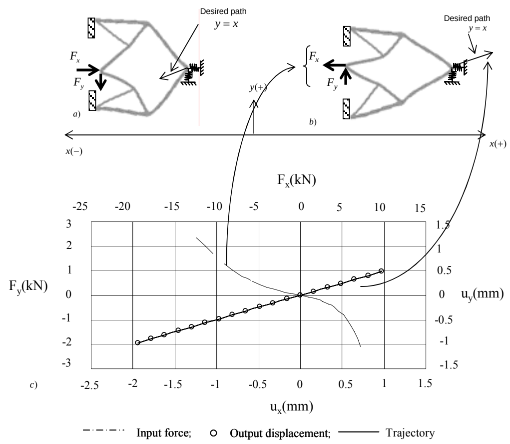

Fig. 13. a) Mechanism when controlled to follow forward inclined path against workpiece springs with stiffness 10^7N/m; and b) when following a backward inclined path; c) graph showing computed relations between the input forces and output displacements.

5. DISCUSSION AND CONCLUSIONS

In this work, a control algorithm within a computational finite deformation analysis framework has been proposed and demonstrated on hinge-free compliant mechanism designs obtained using continuum topology optimization. In the proposed control framework, one solves for the required actuation forces at the mechanism's input port such that the mechanism's output port follows a specified trajectory in an optimal sense. Although many issues remain to be investigated in combined design and control of compliant mechanisms, the concept of using control seems very promising.

6. ACKNOWLEDGEMENTS

This research was funded in part by a grant from the University of Iowa CIFRE program.

7. REFERENCES

[1] Howell, L.L, and Midha, A., 1996, "A Loop-Closer Theory for the Analysis and Synthesis of Compliant Mechanisms," *Journal of Mechanical Design*, **118**, pp. 121-125.

[2] Smith, S. T., 2000, Flexures: Elements of Elastic Mechanisms, Gorden & Breach, Amsterdam.

[3] Howell, L.L., 2001, Compliant Mechanisms, John Wiley & Sons, Inc., New York.

[4] Ananthasuresh, G.K., Kota, S, and Gianchandani, Y., 1994, "A Methodical Approach to the Design of Compliant Micromechanisms," *Solid-State Sensor, Actuator Workshop, South Carolina*, June 13-16.

[5] Sigmund, O., 1997, "On the Design of Compliant Mechanisms Using Topology Optimization," *Mech. of Struct. and Mach.*, **25** (4) , pp. 495-526.

[5] Pedersen, C.B.W., Buhl, T., and Sigmund, O., 2001, "Topology synthesis of large-displacement compliant mechanisms," *Int. J. Num. Meth. Engrg*. **50**, pp. 2683-2705.

[6] Saxena, A., and Ananthasuresh, G.K., 2001, "Topology synthesis of compliant Mechanisms for Nonlinear Force-Deflection and Curved Path Specifications," *J. Mech. Design. ASME*, **123**, pp. 33-42.

[7] Rahmatalla, S.F., and Swan, C.C., 2004, "Sparse monolithic compliant mechanisms using continuum structural topology optimization," in review.

[8] Arora, J.S., 1989, Introduction to Optimum Design, McGraw-Hill, Inc., New York.

[9] Vincent, T.L., and Grantham, W.J., 1997, Nonlinear and Optimal Control Systems, John Wiley & Sons, Inc., New York.

[10] Ciarlet, P. G., 1988, "*Mathematical Elasticity, Volume I: Three-Dimensional Elasticity*", Elsevier, Amsterdam.

[11] Swan, C.C., and Kosaka, I., 1997, "Voigt-Reuss topology optimization for structures with nonlinear material behaviors," *Int. J. Numer. Meth. Engrg*. **40**, 3785-3814.

[12] Rahmatalla, S., and Swan, C.C., 2003, "Continuum topology optimization of buckling-sensitive structures," *AIAA J*. **41**(5), 1180-1189.

[13] Cardoso J.B. and Arora, J.S., 1991, "Adjoint sensitivity analysis for nonlinear dynamic thermoelastic systems," *AIAA J*. **29** (2), 253-263.